J. Fluid Mech. (1984), *vol.* 146, *pp.* 313–330
Printed in Great Britain

An alternative approach to linear and nonlinear stability calculations at finite Reynolds numbers

By F. T. SMITH, D. PAPAGEORGIOU AND J. W. ELLIOTT†
Department of Mathematics, University College London WC1E 6BT

(Received 26 October 1983 and in revised form 25 April 1984)

An extended version of the interactive boundary-layer approach which has been used widely in steady-flow calculations is applied here to the linear and nonlinear stability properties of channel flows and boundary layers in the moderate-to-large Reynolds-number regime. This is the regime of most practical concern. First, for linear stability the agreement found between the interactive approach and Orr–Sommerfeld results remains fairly close even at Reynolds numbers as low as about $\frac{1}{10}$ of the critical value for plane Poiseuille flow, or $\frac{1}{5}$ for Blasius flow. Secondly, nonlinear unsteady calculations and comparisons with full solutions obtained by enlarging the same method are also presented. Overall the work suggests that, at the finite Reynolds numbers where real interest lies, the dominant physical processes of instability in channel flow and boundary layers are of boundary-layer form, with interaction, and it suggests also an alternative numerical technique for determining those processes. This alternative technique uses the interactive boundary-layer method as the central means for obtaining full unsteady Navier–Stokes solutions.

1. Introduction

There seems little doubt that a major need in the understanding of nonlinear hydrodynamic instability and subsequent transition, in boundary layers, channel flows, pipe flows and others, is for more nonlinear computational solutions and accurate properties at finite Reynolds numbers. For, on the one hand, weakly nonlinear theory (see Stuart 1960, 1971; Watson 1960; Stewartson & Stuart 1971), as it is based near a linear neutral solution, is confined conceptually or strictly (if not in reality) to a quite limited range of wavenumbers, Reynolds numbers and disturbance sizes, the degree of that confinement in practice varying from problem to problem and being uncertain usually. On the other, inviscid theory or asymptotic theory (Reid 1965; Tollmien 1929; Schlichting 1933; Lin 1955; Smith 1979*a*; Drazin & Reid 1981) for large Reynolds numbers, or large Taylor, Görtler or Grashof numbers, for instance, likewise has a range of application and assumptions which at first sight at least (see below, however) might appear to be too limited or questionable to be of much practical help. In fact both theories do often 'work' surprisingly well over a much wider range of conditions than might be expected and that is an encouraging aspect. In addition the theories provide much valuable analytical insight into the nature of instability mechanisms as well as allowing some valuable checks to be made on computational results. Yet strictly, and from a perhaps rather pessimistic viewpoint, both these theories and others rely in essence on the assumption of a vanishingly small parameter such as the disturbance energy or the inverse Reynolds number, whereas in practice the values of the parameters of real concern are finite and non-zero. So, despite the undoubted value of these two major

† Present address: Department of Applied Mathematics, The University, Hull HU6 7RX.

analytically based theories in terms of their insight, it would seem that in general they have to be supplemented and extended, or at least tested, by considerable numerical efforts addressing the full Navier–Stokes equations if results of practical interest are to be derived, for sizeable disturbances to a given basic motion. This is not to advocate the superiority of fully computational methods; far from it – we merely conclude that they are most necessary.

Yet traditional methods of numerical solution of the Navier–Stokes equations can often encounter severe difficulties, in accuracy, convergence rates, numerical stability, and computer time and storage, at Reynolds numbers beyond moderate values. Although these types of difficulty can be suppressed in different flow problems by various means (see e.g. Dennis & Hudson 1978; Patera & Orszag 1981; Fornberg 1980; Smith 1981), with varying degrees of success, the question does arise as to whether alternative methods of numerical solution can be constructed which reflect more adequately the principal physical features tending to dominate the flow response as the Reynolds number increases. Moreover the Reynolds numbers of most practical interest are most often in the moderate-to-high range in stability problems. This is particularly so for plane Poiseuille flow through a channel, where the critical Reynolds number of 5772 (in traditional notation) according to linear theory 'looks so large', while the corresponding number in Blasius boundary-layer flow is approximately 520, which is also 'largish'. Even in experiments, the critical Reynolds number for plane Poiseuille flow tends to remain within the 'largish' range 1000–3000 for all but the most carefully controlled conditions. Large-looking critical Reynolds numbers are also a feature of rotating fluid flows, for instance. Of course all these critical values are finite, not asymptotic, and can be lessened in appearance by redefinition of the variables, but then the new variables contain 'largish' numerical values instead, and so the largeness remains present. Can any advantage therefore be taken of the presence of a large or moderate-to-high parameter in the nonlinear unsteady governing equations? Surely such a parameter could reflect the near-emergence of some overriding physical mechanism for increasing Reynolds numbers.

The general 'interactive boundary-layer' approach in its numerous guises at finite Reynolds numbers takes up the above theme. The approach acknowledges, and is guided by, the asymptotic properties of the flow solution for large Reynolds numbers, and bases its computational schemes upon those properties by addressing first, where possible, an appropriate simplified set of equations rather than the complete Navier–Stokes equations. The reduced set is chosen to retain the primary physics of the stability problem in the moderate-to-high Reynolds-number regime as guided by the asymptotic theory; and so, secondly and if necessary, the resultant solution can be restored to 'full' Navier–Stokes status almost as an afterthought, by inclusion of the omitted secondary effects only then (as is done in the present work, see below). The interactive boundary-layer concept has proved very useful in numerical studies of steady flow (see e.g. Davis & Rubin 1980; Davis & Werle 1981; Rubin 1982; and references therein) in aerodynamics and in channel flows. In this paper we consider its application to the linear and nonlinear unsteady flow and instability of boundary layers and channel flows. The concept, which in our view has many guises or extensions (e.g. the parabolized Navier–Stokes equations) and nomenclatures, and which loosely is in the spirit of some classical approximations for linear disturbances, centres around the unsteady nonlinear boundary-layer equations subject to interactive, non-classical, boundary conditions. By incorporating also lateral pressure

gradients it reproduces the asymptotic behaviour of both Navier–Stokes and Orr–Sommerfeld solutions accurately, to several orders of magnitude, as well as allowing weakly or strongly nonlinear amplitude modulations and emergent critical layers to exert their influence at finite Reynolds numbers. The general interactive boundary-layer approach therefore represents perhaps the most *practically* valuable application of the insight which asymptotic theory provides. Asymptotic theory almost always yields increased theoretical and physical understanding anyway, as well as comparisons and initial estimates for calculations, and the flexibility of analytical results; it would seem something of a disservice not to attempt also to create more appropriate numerical schemes for the important moderate-to-large Reynolds-number regime as a result.

Below we consider an extended interactive boundary-layer approach and its origins for unsteady channel flows and boundary layers, in §§2 and 3 in turn, and then present results and comparisons for infinitesimal linear disturbances in §4. Computations for nonlinear disturbances are described in §5, followed by a discussion in §6 on our restoring the results to 'full' status and subsequent comparisons. Finally §7 provides a further discussion. The agreement found between the interactive and the full solutions is quite close even at subcritical Reynolds numbers as low as $\frac{1}{10}$ of the critical linear value for plane Poiseuille flow and $\frac{1}{5}$ for the Blasius boundary layer. In a practical or numerical sense these comparisons, and the associated development of an alternative numerical method addressing the full Navier–Stokes equations in §6, represent the firmest tests on the value of the present interactive concept, and we may regard these as very favourable features from both the computational and the theoretical standpoints. The scope is restricted here to two-dimensional unsteady motions, for an incompressible fluid, with the characteristic Reynolds number R being based on a typical flow speed u_∞ and a typical flow thickness, the channel half-width or a typical boundary-layer displacement thickness. Corresponding non-dimensional velocities u, v, Cartesian coordinates x, y and time t are used, while the pressure is written as $\rho_\infty u_\infty^2 p$, where ρ_∞ is the density of the fluid. For the boundary-layer case the global Reynolds number based on a typical lengthscale of the boundary layer is then $Re \propto R^2$. The subscripts r, i used below denote real and imaginary parts.

2. The concept in channel flow

In support of the extended interactive boundary-layer concept to be adopted for channel flows at finite Reynolds numbers R, we take the nonlinear stability properties (Smith 1979*b*) for asymptotically large R as our starting point.

Based first around the lower branch of the neutral curve, these asymptotic properties take a double-decked interactive form there (Smith 1979*b*; Hall & Smith 1982). In the core of the motion, for $0 < y < 2$, the total flow field has the form

$$(u, v, p) = (\bar{u}(y), 0, 0) + (\epsilon_2 u_1, \epsilon_3 v_1, \epsilon_4 p_1) + \ldots, \tag{2.1}$$

with a large characteristic lengthscale $x = \epsilon_1^{-1} X$ controlling the flow solution, whereas in the viscous wall layer, where $y = \epsilon_2 Y$, the expansion is

$$(u, v, p) = (\epsilon_2 U, \epsilon_5 V, \epsilon_4 P) + \ldots . \tag{2.2}$$

Here $\epsilon_n = R^{-\frac{1}{7}n}$, $n \geqslant 1$, are small parameters and $\bar{u}(y)$ is the basic inflection-free velocity profile, in the channel defined by $0 \leqslant y \leqslant 2$. To be definite we take this to be plane Poiseuille flow, $\bar{u} = y - \frac{1}{2}y^2$, although more general profiles with or without

inflexion points can be accommodated also. The governing equations in the core are, from a formal substitution into the Navier–Stokes equations,

$$\frac{\partial u_1}{\partial X}+\frac{\partial v_1}{\partial y}=0, \qquad \bar{u}\frac{\partial u_1}{\partial X}+v_1\frac{\mathrm{d}\bar{u}}{\mathrm{d}y}=0, \qquad \bar{u}\frac{\partial v_1}{\partial X}=-\frac{\partial p_1}{\partial y}. \tag{2.3a,b,c}$$

Meanwhile in the nonlinear wall layer the Navier–Stokes equations reduce to the boundary-layer equations

$$\frac{\partial U}{\partial X}+\frac{\partial V}{\partial Y}=0, \qquad \frac{\partial U}{\partial T}+U\frac{\partial U}{\partial X}+V\frac{\partial U}{\partial Y}=-\frac{\partial P}{\partial X}+\frac{\partial^2 U}{\partial Y^2}, \qquad 0=-\frac{\partial P}{\partial Y}, \tag{2.4a,b,c}$$

where T denotes the large characteristic timescale, $t=\epsilon_3^{-1}T$. The boundary conditions required are for no slip at $Y=0$, for matching between (2.3*a–c*) as $y\to 0+$ and (2.4*a–c*) as $Y\to\infty$, i.e. interaction, and for appropriate disturbance symmetry at the centreline $y=1$. Thus

$$P(X,T)=p_1(X,0+,T), \quad \lim_{Y\to\infty}(U-Y)=u_1(X,0+,T), \quad p_1(X,1,T)=0. \tag{2.5a,b,c}$$

Consider next the hierarchy of applications of (2.3*a*)–(2.5*c*). The linearized version of (2.4*a–c*), where $U-Y$, V, P are small, coupled with the core properties (2.3*a–c*), yields the classical asymptote for the Orr–Sommerfeld lower branch of the linear neutral curve and its environs. Next, the weakly nonlinear version of (2.4*a–c*) likewise reproduces the asymptote of the weakly nonlinear Stuart–Watson theory as $R\to\infty$. Thirdly, the fully nonlinear version of (2.4*a–c*), solutions of which have yet to be attempted, corresponds to the asymptotic properties of full Navier–Stokes calculations, again as $R\to\infty$.

Yet in all three versions, although the above account gives the formally correct limit as $R\to\infty$, it is sometimes true that numerically close agreement with the corresponding finite-R results occurs only at rather large R, particularly in stability problems,† *unless* higher-order terms in the expansions, here (2.1), (2.2), are also generated. Again, the limit above is confined to the structure of the lower-branch solutions. A separate limit and its higher-order terms have to be invoked to cover the upper branch, which is considered later in this section and is physically distinct, although there are some hybrid analyses attempting to cover both branches. These two possible criticisms, concerning the practical necessity of higher-order analysis and the awkward distinction between the lower- and upper-branch structures, are dealt with quite competently by the extended interactive boundary-layer approach. This approach simply addresses the equations

$$\frac{\partial u}{\partial x}+\frac{\partial v}{\partial y}=0; \tag{2.6a}$$

$$\frac{\partial u}{\partial t}+u\frac{\partial u}{\partial x}+v\frac{\partial u}{\partial y}=-\frac{\partial p}{\partial x}+\frac{1}{R}\frac{\partial^2 u}{\partial y^2}+\text{`0'}, \tag{2.6b}$$

$$\frac{\partial v}{\partial t}+u\frac{\partial v}{\partial x}+\text{`0'}=-\frac{\partial p}{\partial y}+\text{`0'}+\text{`0'}, \tag{2.6c}$$

† In steady motions, by contrast, qualitative and quantitative agreement between asymptotic theory and finite-R calculations, and with experiments, does occur often at surprisingly moderate or low R (for examples see Messiter 1979; Stewartson 1981; Smith 1982), although there are minor counter-examples to this.

for $0 \leqslant y \leqslant 2$, at finite R. This set, reduced from the Navier–Stokes equations, clearly reproduces the leading-order limits (2.3*a–c*), (2.4*a–c*) when analysed for large R, as we should wish, but it also agrees with the Navier–Stokes equations as regards the higher-order terms (+ ...) in (2.1), (2.2), to several orders of magnitude. For the terms deliberately omitted in (2.6*a–c*) and denoted by + '0' there, i.e. the lateral diffusion $\partial^2 v/\partial y^2$, the streamwise diffusion $\partial^2 u/\partial x^2$, $\partial^2 v/\partial x^2$ and the inertia force $v\,\partial v/\partial y$, affect the expansions (2.1), (2.2) only at relative orders of ϵ_2, ϵ_4 respectively at most. Thus the set (2.6*a–c*) should capture the structure, and hence the dominant physics, of the lower branch's nonlinear stability features well. Moreover it provides the desired unified approach, since it captures also the upper branch's linear and nonlinear stability features, as follows.

Around the upper branch of the linear or nonlinear neutral curve for large R (Smith 1979*b*; Smith & Gajjar 1984) the main streamwise lengthscale is again long, $x = \Delta_1^{-1} X$, where Δ_n ($\ll 1$) denotes $R^{-\frac{1}{11}n}$. The unsteady flow structure there has a quadruple-decked form, comprising a predominantly inviscid core again, and a mainly inviscid wall layer of thickness Δ_2 within which are two distinct viscous zones, the Stokes wall layer and the critical layer. The timescale is again long, $t = \Delta_3^{-1} T$. Without needing to go into the detailed expansions, we observe that the core is controlled again by equations of the form (2.3*a–c*), and so is the inviscid wall layer in fact, although the next-order contribution bringing in $\bar{u}''$ plays an important role there in producing a weak logarithmic irregularity at the critical level. Here the viscous critical layer, whether linear, weakly nonlinear or fully nonlinear, and whether in or out of a neutral state (Smith & Gajjar 1984), has thickness $\Delta_{\frac{19}{3}}$ and has the property that the pressure variation across it laterally is negligible and the main viscous term comes from $\partial^2 u/\partial y^2$, as in (2.6*b*). Airy's equation or its nonlinear/unsteady counterpart for the dominant vorticity $\partial u/\partial y$ smooths out the logarithmic irregularity, produces a velocity jump across the critical layer, and is obtained identically from both (2.6*a–c*) and the Navier–Stokes equations. Similarly, the Stokes wall layer of thickness Δ_4 required for the satisfaction of the no-slip condition at $y = 0$ emerges in the same form from the Navier–Stokes equations and from (2.6*a–c*), again to several orders of magnitude. We observe further that any nonlinearity (Bodonyi & Smith 1981; Smith & Bodonyi 1982) affects the critical layer most, leaving the flow structure elsewhere intact until the disturbance lengthscale shortens significantly. Indeed a hierarchy of applications much like that for the lower branch describes the linear and nonlinear effects of the upper-branch type.

Given that the reduced, unified, set (2.6*a–c*) reproduces the correct asymptotic behaviour on and around both the branches of the neutral curve and in-between, to several orders, then, we investigate finite-R features and comparisons in §4 below, after a discussion of boundary-layer stability in §3.

3. The concept in boundary-layer flows

Reasoning akin to that in §2 applies also to the linear and nonlinear instability of inflection-free boundary-layer profiles $\bar{u}(y)$, apart from one possible extra feature below. Profiles with inflection points can also be accommodated nevertheless: see later comments.

Thus the lower branch and its environs, for both linear and nonlinear disturbances, are controlled at large R by the triple-deck interactive structure (Smith 1979*a*), in which the governing equations for the lower deck nearest the wall are (2.4*a–c*). Here,

apart from the finite non-zero skin-friction factor $\bar{u}'(0)$, the expansion of the flow solution is

$$(u, v, p) = (\epsilon_1 U, \epsilon_3 V, \epsilon_2 P) + \ldots \tag{3.1}$$

now, with $\epsilon_n \equiv R^{-\frac{1}{4}n} \ll 1$, $x = \epsilon_1^{-1} X$ is large, $y = \epsilon_1 Y$ is small and time $t = \epsilon_2^{-1} T$ is large. The main deck, the majority of the boundary layer, likewise yields (2.3*a*, *b*), but (2.3*c*) is replaced by $\partial p_1/\partial y = 0$, giving $p_1 = P(X, T)$, where

$$(u, v, p) = (\bar{u}(y), 0, 0) + (\epsilon_1 u_1, \epsilon_2 v_1, \epsilon_2 p_1) + \ldots . \tag{3.2}$$

The possible extra feature arising, and referred to above, concerns the potential flow outside the boundary layer, in the upper deck. There the pressure disturbance satisfies Laplace's equation, since $y = \epsilon_1^{-1} \bar{y}$ is then comparable to x, and $\bar{u}$ is effectively unity. So the extended interactive boundary-layer equations (2.6*a–c*) are in principle still appropriate within the upper deck. This, however, is predominantly inviscid anyway, being controlled to leading order by the potential-flow problem

$$\left(\frac{\partial^2}{\partial X^2} + \frac{\partial^2}{\partial \bar{y}^2}\right) \bar{p}_2 = 0, \tag{3.3a}$$

with

$$\left.\begin{aligned} &\bar{p}_2 = P(X, T), \\ &\frac{\partial \bar{p}_2}{\partial \bar{y}} = -\frac{\partial v_1}{\partial X}(X, \infty, T) \end{aligned}\right\} \quad \text{at} \quad \bar{y} = 0+, \tag{3.3b, c}$$

to match (3.2), and a boundedness condition in the far field. Here $p = \epsilon_2 \bar{p}_2$, and $u = 1 + \epsilon_2 \bar{u}_2$, $v = \epsilon_2 \bar{v}_2$, to leading orders. Hence for convenience we may restrict the interactive boundary-layer version (2.6*a–c*) to the viscous boundary layer itself, the lower and main decks, provided that the outer condition imposed on (2.6*a–c*) as $y \to \infty$ reflects the match with the potential flow (3.3) outside. Accuracy, in comparison with the full Navier–Stokes equations, is then maintained to several levels of order ϵ_n (as in §2) by (2.6*a–c*) within the boundary layer, while outside also the accuracy level can be improved by extending (3.3*c*) to include the time derivative of the displacement δ as described below. The restriction of (2.6*a–c*) here to the boundary-layer region in essence reduces the extent of the domain of integration. The equations (2.6*a–c*) could still be solved outside the boundary layer as well, but by limiting the integration to the boundary-layer region and using interaction with (3.3*a–c*) outside we keep the grid extent down and avoid more multistructured numerical difficulties arising at higher Reynolds numbers. This aspect of course is perhaps rather a matter of choice, interpretation of the asymptotics or guesswork, as are several aspects in this paper, and other workers may prefer different treatments. Our aim here and throughout is to be useful and realistic and to enlarge the scope of the asymptotic knowledge rather than just being asymptotically correct. However, the major test ultimately, aside from truncation and roundoff error, is the comparison with full solutions (Navier–Stokes or Orr–Sommerfeld), and there the present interactive version does do well, even at relatively low Reynolds numbers, as we shall see subsequently in §§4 and 6. That in a sense gives the justification for the present approach.

So we couple (2.6*a–c*) for finite Reynolds numbers R with the outer inviscid problem

$$\left(\frac{\partial^2}{\partial x^2} + \frac{\partial^2}{\partial y^2}\right) p = 0, \tag{3.4}$$

by means of the conditions

$$\psi \sim u^* y - \delta \quad \text{in (2.6}a\text{–}c\text{)} \quad \text{as} \quad y \to \infty \tag{3.5a}$$

$$\left.\begin{aligned} -\frac{\partial p}{\partial x} &= \frac{\partial u^*}{\partial t} + u^* \frac{\partial u^*}{\partial x}, \\ -\frac{\partial p}{\partial y} &= \frac{\partial^2 \delta}{\partial x\, \partial t} + u^* \frac{\partial^2 \delta}{\partial x^2} \end{aligned}\right\} \quad \text{in (3.4)}, \quad \text{as} \quad \alpha y \to 0+. \tag{3.5b, c}$$

Here (3.5*a*–*c*), with u^*, δ, p unknown, are consistent formally with the Navier–Stokes equations and matching at large R, to several orders of magnitude again. At finite R no formal consistency exists, of course, but the hope, as explained in §1 and to be tested subsequently, is that numerical accuracy is preserved because of the emphasis on the major physical balances operating.

It can be verified that (2.6*a*–*c*) coupled with (3.4), (3.5*a*–*c*) also allows the correct upper-branch asymptotes to emerge. These asymptotes (Bodonyi & Smith 1981) depend more on the particular form of the boundary-layer profile, in linear or nonlinear stability, but in any case the asymptotic structure divides into four zones dominated by the viscous or inviscid boundary-layer equations and one outermost zone of potential-flow properties. So again either the coupling/interaction of (2.6*a*–*c*) with (3.4), (3.5*a*–*c*), or just (2.6*a*–*c*) acting across the entire flow, is sufficient to capture the upper-branch stability features to a number of orders of magnitude. Hence an unified treatment covering the whole neutral curve, whether linear or nonlinear, and whether in neutral conditions or not, is in prospect.

4. Linear stability properties

The first most obvious test to make on the extended interactive boundary-layer approach put forward in §§2 and 3 is to compare its predictions with 'full' Orr–Sommerfeld ones for linear disturbance properties. This was done as follows. For an infinitesimal disturbance size A_0, if a travelling-wave perturbation of the form

$$(u, v, p) = (\bar{u}(y), 0, 0) + A_0 \operatorname{Re}(\tilde{u}, \tilde{v}, \tilde{p})\, \mathrm{e}^{\mathrm{i}(\alpha x - \beta t)} + O(A_0^2) \tag{4.1}$$

is assumed (see also comments in §5), then at finite R the resultant linearized form of the Navier–Stokes equations is

$$\mathrm{i}\alpha \tilde{u} + \tilde{v}' = 0, \tag{4.2a}$$

$$\mathrm{i}\alpha\left(\bar{u} - \frac{\beta}{\alpha}\right)\tilde{u} + \tilde{v}\bar{u}' = -\mathrm{i}\alpha\tilde{p} + R^{-1}(\tilde{u}'' - \alpha^2\tilde{u}), \tag{4.2b}$$

$$\mathrm{i}\alpha\left(\bar{u} - \frac{\beta}{\alpha}\right)\tilde{v} = -\tilde{p}' + R^{-1}(\tilde{v}'' - \alpha^2\tilde{v}) \tag{4.2c}$$

for $(\tilde{u}, \tilde{v}, \tilde{p})(y)$, or the Orr–Sommerfeld equation

$$\left(\bar{u} - \frac{\beta}{\alpha}\right)(\tilde{\psi}'' - \alpha^2\tilde{\psi}) - \bar{u}''\tilde{\psi} = \frac{1}{\mathrm{i}\alpha R}(\tilde{\psi}^{\mathrm{iv}} - 2\alpha^2\tilde{\psi}'' + \alpha^4\tilde{\psi}) \tag{4.2d}$$

for the stream function $\tilde{\psi}(y)$. Here the wavenumber α is assumed real, the complex

frequency β is taken to be the unknown eigenvalue, and $\tilde{u} = \tilde{\psi}'(y)$, $\tilde{v} = -\mathrm{i}\alpha\tilde{\psi}$. The boundary conditions are

$$\tilde{u} = \tilde{v}(= \tilde{\psi} = \tilde{\psi}') = 0 \quad \text{at} \quad y = 0, y_2, \tag{4.2e}$$

where $y_2 = 2$ for the channel flow but $y_2 = '\infty'$ in effect for the boundary layer.

The corresponding linearization of the extended interactive boundary-layer equations (2.6*a–c*) is

$$\mathrm{i}\alpha\tilde{u} + \tilde{v}' = 0, \quad \mathrm{i}\alpha\left(\bar{u} - \frac{\beta}{\alpha}\right)\tilde{u} + \tilde{v}\bar{u}' = -\mathrm{i}\alpha\tilde{p} + R^{-1}\tilde{u}'', \quad \mathrm{i}\alpha\left(\bar{u} - \frac{\beta}{\alpha}\right)\tilde{v} = -\tilde{p}', \tag{4.3a,b,c}$$

or, in terms of $\tilde{\psi}$,

$$\left(\bar{u} - \frac{\beta}{\alpha}\right)(\tilde{\psi}'' - \alpha^2\tilde{\psi}) - \bar{u}''\tilde{\psi} = \frac{1}{\mathrm{i}\alpha R}\tilde{\psi}^{\mathrm{iv}}. \tag{4.3d}$$

These are subject again to (4.2*e*) in the case of channel flow, whereas for the boundary layer we have

$$\left.\begin{aligned} &\tilde{\psi} \sim \tilde{u}^* y - \tilde{\delta}, \quad \tilde{u} \to \tilde{u}^*, \\ &\left(1 - \frac{\beta}{\alpha}\right)\tilde{u} \to -\tilde{p}, \\ &\tilde{p} \to -(\alpha - \beta)\tilde{\delta} \end{aligned}\right\} \quad \text{as} \quad y \to y_2, \tag{4.3e}$$

in view of (3.4), (3.5*a–c*), with $\tilde{u}^*$ ($\equiv (u^* - 1)/A_0$, see (3.5*b*, *c*)) being an unknown finite constant. In (4.3*e*) strictly y_2 should be large, but not αy_2, in order that the exp ($\pm\alpha y$) behaviour associated with solutions of (4.2*d*), (4.3*d*) as $\alpha y \to \infty$ is deliberately not achieved. This corresponds to solving within the boundary layer alone (the main and lower decks) and leaving the flow outside (in the upper deck) accounted for by (3.4), with (3.5*b*, *c*) and with αy there being $O(1)$ as explained in §3. This is strictly valid only asymptotically, but as we shall see it turns out also to 'work' in the numerical sense at the finite Reynolds numbers R of real interest, and that is the ultimate test in the present context, leaving aside the effects of truncation and roundoff error. Additionally in (4.3*e*) the final condition relating $\tilde{p}$, $\tilde{\delta}$ is the interactive one; for outside the boundary layer the solution of (3.4) with (4.1) yields $p \propto A_0\tilde{p}\,\mathrm{e}^{-\alpha y}$, so that (3.5*c*) then requires $\alpha\tilde{p} = \alpha\beta\tilde{\delta} - \alpha^2\tilde{\delta}$ because $u^* = 1 + O(A_0)$, and we then have (4.3*e*), to leading orders. Note also that here the interactive version (4.3*d*) amounts to a long-wave (small-α) approximation of the full equation (4.2*d*), but only as far as the viscous terms are concerned. This makes good physical and theoretical sense, for viscous terms matter much only in relatively thin layers (of scale $[y] \ll 1$) at large R anyway. So the influence of the neglected orders $\alpha^2[y]^2$ in the viscous terms is then correspondingly diminished, compared with the relative orders α^2 which are kept elsewhere in the equations. Conversely, in the boundary-layer case it should be clear from our earlier comments, especially those in §3, that the α^2 terms kept are significant structurally or actively only outside the boundary layer, not within it. The α^2 terms within the boundary layer influence the solution only as passive numerical corrections, so that in particular the exp ($\pm\alpha y$) behaviour referred to above is avoided since αy does not become large. Further comments concerning the level of accuracy of (4.3*d*) compared with (4.2*d*), at large R, are covered by the earlier remarks in §§2 and 3 on the nonlinear versions. More important for our present purposes are the results achieved at finite R-values of interest, where a direct comparison between the full set (4.2*d*) and the reduced, interactive version (4.3*d*) can be made, thus providing the necessary test on the usefulness of the interactive version.

Numerical solutions were obtained by means of a fairly straightforward finite-difference scheme. More sophisticated differencing or iteration or other numerical devices could be used at this stage, but that is not the main point here; our prime concern instead is in the value and accuracy of the interactive equations as compared with the full ones. We preferred to address the forms (4.2*a–c*), (4.3*a–c*) for velocities and pressure, rather than (4.2*d*), (4.3*d*) for the stream function. Thus for (4.2*a–c*) we discretized the equations in the form

$$\tfrac{1}{2}\mathrm{i}\alpha(\tilde{u}_j+\tilde{u}_{j-1})+\frac{\tilde{v}_j-\tilde{v}_{j-1}}{\Delta y}=0 \quad \text{for} \quad 2\leqslant j\leqslant J, \tag{4.4a}$$

$$\mathrm{i}\alpha\left(\bar{u}-\frac{\beta}{\alpha}\right)\tilde{u}_j+\tilde{v}_j\,\bar{u}'=-\mathrm{i}\alpha\tilde{p}_j+R^{-1}\left[\frac{\tilde{u}_{j+1}-2\tilde{u}_j+\tilde{u}_{j-1}}{(\Delta y)^2}-\alpha^2\tilde{u}_j\right] \quad \text{for} \quad 2\leqslant j\leqslant J-1, \tag{4.4b}$$

$$\tfrac{1}{2}\mathrm{i}\alpha\left(\bar{u}-\frac{\beta}{\alpha}\right)(\tilde{v}_j+\tilde{v}_{j-1})=-\frac{\tilde{p}_j-\tilde{p}_{j-1}}{\Delta y}+R^{-1}\left[-\mathrm{i}\alpha\left(\frac{\tilde{u}_j-\tilde{u}_{j-1}}{\Delta y}\right)-\tfrac{1}{2}\alpha^2(\tilde{v}_j+\tilde{v}_{j-1})\right] \quad \text{for} \quad 2\leqslant j\leqslant J. \tag{4.4c}$$

Here $J-1$ is the number of steps in y, $(J-1)\,\Delta y=y_2$ fixes the steplength Δy for a finite value of y_2, while $\tilde{u}_j$ stands for $\tilde{u}[(j-1)\,\Delta y]$ and so on. In (4.4*b*, *c*) $\bar{u}$ is evaluated at $y=(j-1)\,\Delta y$, $y=(j-\frac{3}{2})\,\Delta y$ respectively, and similarly for $\bar{u}'$, so that nominal second-order accuracy in Δy holds throughout. The constraints

$$\tilde{u}_1=\tilde{v}_1=\tilde{u}_J=\tilde{v}_J=0 \tag{4.4d}$$

replace (4.2*e*), and a normalization

$$\tilde{p}_1=1 \tag{4.4e}$$

is made. Hence (4.4*a–e*) provide $3J+1$ nonlinear complex equations for the $3J+1$ complex unknowns $\tilde{u}_j$, $\tilde{v}_j$, $\tilde{p}_j$ $(1\leqslant j\leqslant J)$ and β, for a prescribed value of α. Newton iteration converts these to linear form, with the associated matrix being block double-diagonal and each block being 3×3. Matrix inversion was then performed by Gaussian elimination, to determine the Newton increments, and the iterations were continued until the successive values of each of the unknowns above differed by less than 10^{-7}. Typically this took about 4 iterations. For the interactive version (4.3*a–c*) the same approach was used, with the term involving α^2 in (4.4*b*), and the viscous terms in (4.4*c*), simply replaced by zero. Values of J between 101 and 401 and, in the boundary-layer case, of y_2 between 20 and 160, were used to check on the numerical accuracy achieved. In the interactive version, however, it proved sufficient to keep y_2 smaller, at a value of 10 or 20, for the required accuracy in the boundary-layer case where (4.3*e*) is invoked at $j=J$. We believe the overall accuracy achieved is at least graphical, which suffices in the present context, although it can be improved readily by means of grid refinement and by grid stretching for example. Comparisons of the results with those from other computational techniques bear out the accuracy obtained here, as well as the robustness of the method.

Figure 1 shows the results for β_r, β_i as functions of α, for plane Poiseuille flow, over a range of Reynolds numbers R between 500 and 7000. This is about the range of most practical interest, since the critical R of linear Orr–Sommerfeld theory is approximately 5772, whereas experimentally instability is found usually for R much lower, 1000–3000, unless the experiment is very controlled to minimize the disturbances present. The results from the full and the interactive methods agree reasonably well, and indeed surprisingly so, over the whole range covered, with the agreement

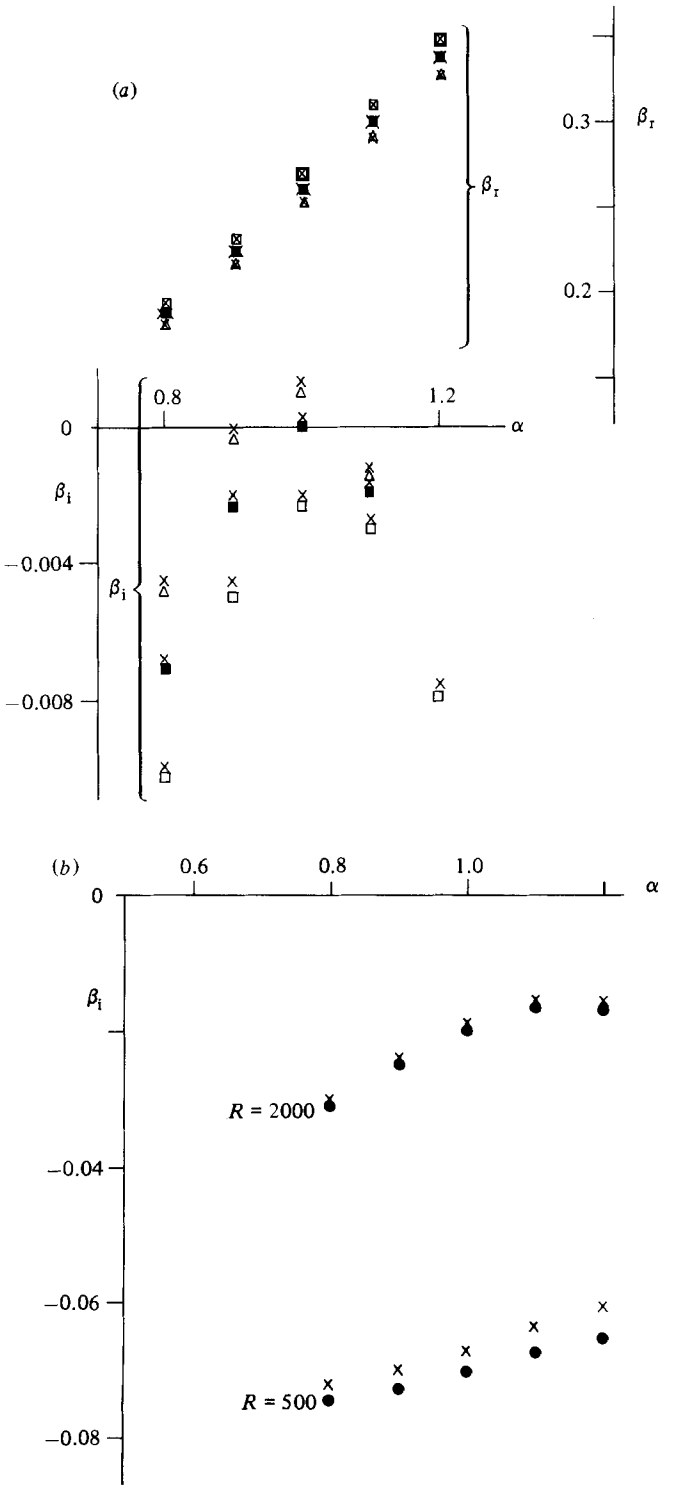

FIGURE 1. For the linear stability of plane Poiseuille flow, comparisons between interactive and full Orr–Sommerfeld solutions (see §§2, 4) for β_r, β_i versus α: (*a*) △, ■, □ give full solutions at $R = 7000$, 6000, 5000 respectively and × give corresponding interactive results; (*b*) ● give full solutions, × give interactive ones, for $R = 2000$ and 500 as shown.

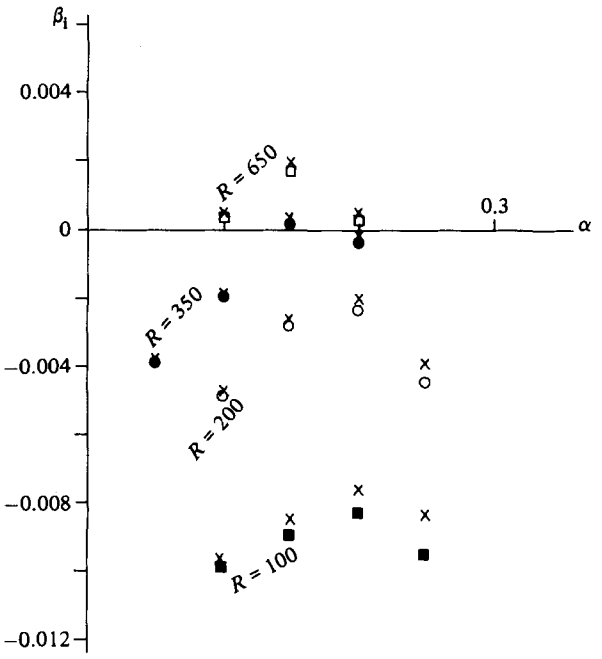

FIGURE 2. Comparisons between interactive and full solutions for β_i versus α in the linear stability of the Blasius boundary layer (see §§3, 4). Full solutions at $R = 650$, 350, 200, 100 are marked by symbols □, ●, ○, ■ respectively, with × giving the corresponding interactive results.

improving as R increases, as should be expected. Even for R as low as 500, however, the agreement is typically to within approximately 1 % in β_r and 4 % in β_i. Around the linear neutral curve these typical differences diminish to less than approximately $\frac{1}{4}$%, 2 % respectively, so that the interactive approach reproduces the entire neutral curve very well.

For the Blasius boundary layer the results for β_i from the two methods are given in figure 2. The Reynolds-number range $100 \leqslant R \leqslant 650$ is covered, thus straddling the linear critical value of $1.720R \approx 520$. Percentage differences obtained are comparable to those of figure 1, despite the much lower range of R-values studied. It is interesting to note that if we reduce the equation set (4.3) further by setting $\partial p/\partial y$ to be zero within the boundary layer, as leading-order theory would suggest asymptotically, then the differences at finite R become more pronounced. This ties in with the comment earlier in this section (second paragraph) relating to the long-wave approximation applied to viscous terms only.

The fact that the extended interactive concept continues to be of practical value not only above, but also well below, the critical value of R in linear theory is encouraging. We therefore move on to nonlinear properties.

5. Nonlinear stability properties

The fully nonlinear unsteady set (2.6*a–c*) now merits study in view of the encouraging comparisons found above for linear theory and of the overriding need for nonlinear stability features at finite R, away from the linear neutral curve, as mentioned in §1. We obtained nonlinear numerical solutions of (2.6*a–c*) for channel flow by using the following spectral method, which is built on the methods described in §4.

Spatial periodicity in x, of wavelength $2\pi/\alpha$, is assumed, so that Fourier series of the form

$$(u, \psi) = (u_0, \psi_0) + \sum_{n=1}^{\infty} [u_n, \psi_n) E^n + (\hat{u}_n, \hat{\psi}_n) E^{-n}], \tag{5.1a}$$

$$p = \sum_{n=0}^{\infty} (p_n E^n + \hat{p}_n E^{-n}) + xQ(t) \tag{5.1b}$$

apply for all $t > 0$. Here ψ is the stream function, $\hat{}$ denotes the complex conjugate, and u_n, ψ_n, p_n are unknown, generally complex, functions of y, t. The function $Q(t)$ of t is unknown and real, u_0, ψ_0 are also unknown and real, and

$$E \equiv \exp(\mathrm{i}\alpha x). \tag{5.1c}$$

Formal substitution into the extended interactive boundary-layer equations (2.6a–c) (cf. §6) therefore leaves, after some rearrangement, the component equations

$$u_n = \frac{\partial \psi_n}{\partial y} \quad \text{for} \quad n \geqslant 0, \tag{5.2a}$$

$$\frac{\partial u_n}{\partial t} + \mathrm{i}(n\alpha)\left[u_0 u_n - \psi_n \frac{\partial u_0}{\partial y} + p_n\right] - \frac{1}{R}\frac{\partial^2 u_n}{\partial y^2} = \mathscr{L}_n \quad \text{for} \quad n \geqslant 1, \tag{5.2b}$$

$$\frac{\partial u_0}{\partial t} + Q(t) - \frac{1}{R}\frac{\partial^2 u_0}{\partial y^2} = \mathscr{L}_0, \tag{5.2c}$$

$$-\mathrm{i}(n\alpha)\frac{\partial \psi_n}{\partial t} + (n\alpha)^2 u_0 \psi_n + \frac{\partial p_n}{\partial y} = \mathscr{M}_n \quad \text{for} \quad n \geqslant 1, \tag{5.2d}$$

$$2\frac{\partial p_0}{\partial y} = \mathscr{M}_0, \tag{5.2e}$$

where the right-hand sides $\mathscr{L}_n$, $\mathscr{M}_n$ are given by

$$\begin{aligned} \mathrm{i}\alpha^{-1}\mathscr{L}_n = {} & \sum_{m=1}^{n-1}\left[(n-m)u_m u_{n-m} - m\psi_m \frac{\partial u_{n-m}}{\partial y}\right] \\ & + \sum_{m=1}^{\infty}\left[(m+n)\hat{u}_m u_{m+n} + m\hat{\psi}_m \frac{\partial u_{m+n}}{\partial y}\right] \\ & + \sum_{m=n+1}^{\infty}\left[(n-m)u_m \hat{u}_{m-n} - m\psi_m \frac{\partial \hat{u}_{m-n}}{\partial y}\right], \end{aligned} \tag{5.3a}$$

$$\mathrm{i}\alpha^{-1}\mathscr{L}_0 = \sum_{m=1}^{\infty} m\left(\hat{\psi}_m \frac{\partial u_m}{\partial y} - \psi_m \frac{\partial \hat{u}_m}{\partial y}\right), \tag{5.3b}$$

$$\begin{aligned} -\alpha^{-2}\mathscr{M}_n = {} & \sum_{m=1}^{n-1}(n-m)^2 u_m \psi_{n-m} + \sum_{m=n+1}^{\infty}(m-n)^2 u_m \hat{\psi}_{m-n} \\ & + \sum_{m=1}^{\infty}(m+n)^2 \hat{u}_m \psi_{m+n}, \end{aligned} \tag{5.3c}$$

$$-\alpha^{-2}\mathscr{M}_0 = \sum_{m=1}^{\infty} m^2(u_m \hat{\psi}_m + \hat{u}_m \psi_m), \tag{5.3d}$$

in turn, and $\mathscr{L}_n$, $\mathscr{M}_n$ contain nonlinear contributions.

The component equations are written in the forms (5.2a–e) to indicate the implicit time-marching numerical procedure used for their solution. Second-order finite-difference representations of the left-hand sides are taken as in §4, for the y-derivatives,

with centring at j, $j-\frac{1}{2}$ as appropriate and at time $t+\frac{1}{2}\Delta t$, where Δt is the timestep. Second-order finite-differencing is applied also to the right-hand sides, as described subsequently. With the solution for ψ_n, u_n, p_n for all n known at time t, a first guess is made for the corresponding values at the next timestep $t+\Delta t$. For each value of n, (5.2*a–e*) are then solved, together with the no-slip conditions

$$u_n = \psi_n = 0 \quad \text{at} \quad y = 0, 2 \quad (\text{for } n \geqslant 1) \tag{5.4a}$$

and (5.5) below (for $n = 0$), to give updated values of ψ_n, u_n, p_n at time $t+\Delta t$, with the other components ψ_m, $m \neq n$, etc., kept at their latest stored values. This is done in turn for all n-values and then repeated until all successive iterates are sufficiently close in value. The scheme then moves on to the next timestep. In solving (5.2*a–e*) for ψ_n, u_n, p_n for $n \geqslant 1$, at $t+\Delta t$, we adopted the procedure used in §4 for linear theory, adding in the nonlinear terms $\mathscr{L}_n$, $\mathscr{M}_n$, replacing α by $n\alpha$ as appropriate, and finite-differencing the time derivatives at $t+\frac{1}{2}\Delta t$ in the form

$$\left(\frac{\partial u_n}{\partial t}\right)_j \approx \frac{1}{\Delta t}[u_{nj}(t+\Delta t) - u_{nj}(t)], \tag{5.4b}$$

and similarly for $\partial\psi_n/\partial t$, to produce an effective $\beta = \mathrm{i}/\Delta t$. For ψ_0, u_0, Q, however, a separate approach was taken. The heat-conduction equation (5.2*c*) for u_0 was set in three-point difference form, which, with the boundary conditions $u_0 = 0$ at $y = 0, 2$, yielded a tridiagonal system, readily inverted to give u_{0j} for a given guessed value of $Q(t+\Delta t)$. Then ψ_0 was obtained by integration of (5.2*a*), with $\psi_0 = 0$ at $y = 0$. This left the ψ_0 value incorrect at $y = 2$, but a double iteration with respect to $Q(t+\Delta t)$, revising u_0, restored the required conditions

$$\left.\begin{aligned} u_0 = \psi_0 = 0 \quad &\text{at} \quad y = 0, \\ u_0 = 0, \quad \psi_0 = \tfrac{4}{3} \quad &\text{at} \quad y = 2. \end{aligned}\right\} \tag{5.5}$$

Here (5.5) corresponds to a condition of fixed mass flux. The alternative condition of a fixed pressure gradient remains to be investigated. The right-hand sides $\mathscr{L}_n$ above were differenced with the forms

$$\left.\begin{aligned} u_m u_{n-m} &\approx u_{mj} u_{n-mj}, \\ \psi_m \frac{\partial u_{n-m}}{\partial y} &\approx \psi_{mj} \frac{u_{n-mj+1} - u_{n-mj-1}}{2\Delta y}, \end{aligned}\right\} \tag{5.6a}$$

and so on, for centring at j, whereas in $\mathscr{M}_n$ we took

$$u_m \psi_{n-m} \approx \tfrac{1}{4}(u_{mj} + u_{mj-1})(\psi_{n-mj} + \psi_{n-mj-1}), \tag{5.6b}$$

and so on, for the appropriate centring at $j-\frac{1}{2}$. Again, (5.2*e*) served to determine the pressure component p_0 once the numerical solution for ψ_m, u_m, $m \geqslant 0$, had converged at a given time level. The final point here is that the infinite coupled system (5.2*a–e*) was truncated to a finite, N-component, system by requiring in effect that $\psi_n = u_n = p_n = 0$ for $n > N$.

Typical values taken in the computations were $N = 7$, with $\Delta y = 0.02$, $\Delta t = 0.08$, and an iterative tolerance per timestep of 10^{-6}. This needed about 5–10 iterations. Checks made on the effects of N, Δy, Δt showed that reducing N to 5 altered the results by approximately 7 % over a typical time range of 12, while doubling Δy had about a 5 % effect, and doubling Δt produced about a 1 % influence. Conversely an increase of N to 9, or a halving of Δy or Δt, produced corresponding changes of $\frac{1}{2}$ %, less than 2 %, and $\frac{1}{2}$ % respectively. So the typical values noted above seemed a reasonable choice: see also a further check later. In more detail, for $R = 6000$ and initial

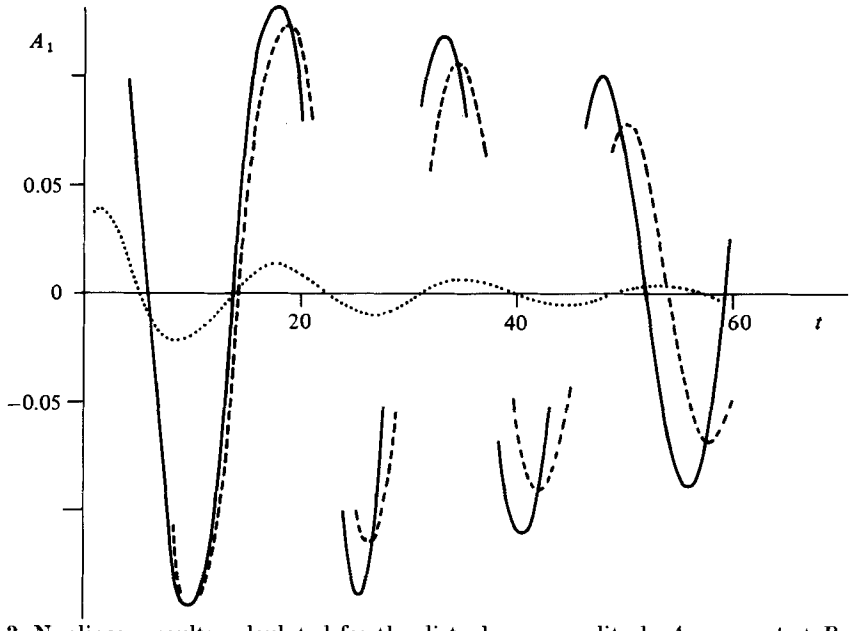

FIGURE 3. Nonlinear results calculated for the disturbance amplitude A_1 versus t at $R = 1000$ in channel flow: . . . . . , initial disturbance size $A = 1$, interactive solution; ——, $A = 5$, interactive; -------, $A = 5$, 'full' solution. See §§ 5, 6.

amplitude $A = 1$ the values obtained at time $t = 12$ for the response A_1 defined below were -0.014758, -0.015758, -0.016067, with $(\Delta y, \Delta t) = (0.04, 0.08)$, $(0.02, 0.04)$, $(0.01, 0.02)$ in turn. These results conform satisfactorily with the second-order accuracy of the scheme used. Also for $(\Delta y, \Delta t) = (0.04, 0.16)$ the corresponding value of A_1 obtained was -0.014824, which provides a check on the effect of the timestep alone.

The initial values used to start the calculations at $t = 0$ were defined by

$$\psi_n = \frac{A(1+\mathrm{i})\, y^2(2-y)^2}{(n+1)^5}, \qquad p_n = \frac{A(1+\mathrm{i})\, y}{(n+1)^5}, \tag{5.7}$$

with (5.2a) for u_n, for $n \geqslant 1$, while u_0, ψ_0 took the plane Poiseuille values $u_0 = y(2-y)$, $\psi_0 = y^2 - \frac{1}{3}y^3$. The computations were performed for various prescribed values of the Reynolds number R, the wavenumber α and the initial amplitude factor A.

The main results so far are presented in figures 3–5, are restricted to $\alpha = 1$ and show a representative unsteady amplitude response $A_1(t)$ of the flow solution given by

$$A_1(t) = \psi_{1r}(0.8, t). \tag{5.8}$$

More comments on these results are given in §6.

6. Raising the nonlinear calculations to 'full' status

The major aim in most interactive boundary-layer approaches at finite R is a numerical one, to provide a close approximation to the full solution by solving accurately the reduced set of equations: here 'full' refers to the solution of the discretized Navier–Stokes equations. A test on the closeness between interactive and full solutions is therefore desirable. Such a test has been given already in §4 for linear disturbances, suggesting a fairly affirmative degree of agreement. In this section a

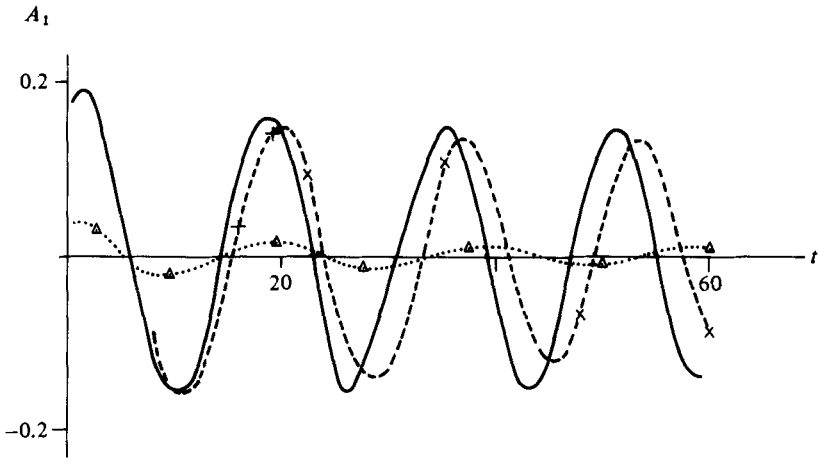

FIGURE 4. Nonlinear disturbance response A_1 versus t at $R = 3000$ in channel flow: . . . . . , $A = 1$, interactive solution; △, $A = 1$, 'full' solution; ——, $A = 5$, interactive; - - - - - - -, $A = 5$, 'full'; ×, $A = 5$, full, but number N of components reduced to 5; +, $A = 5$, full, but N increased to 9. See §§5, 6.

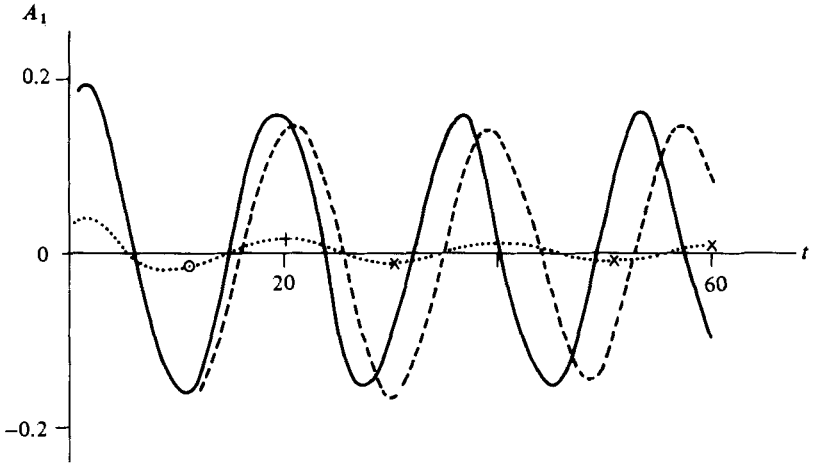

FIGURE 5. Nonlinear disturbance response A_1 versus t at $R = 6000$ in channel flow: . . . . . , $A = 1$, interactive solution; ×, $A = 1$, interactive but timestep Δt doubled; +, $A = 1$, interactive but time and spatial steps Δt, Δy halved; ○, $A = 1$, interactive but Δt, Δy halved again; ——, $A = 5$, interactive; - - - - - - -, $A = 5$ 'full' solution. See §§5, 6.

test applied to the nonlinear results is described, as well as a new means of deriving full Navier–Stokes solutions based on the interactive method of §5.

If we address the Navier–Stokes rather than the extended interactive boundary-layer equations, then the extra contributions from the terms $R^{-1}\partial^2 u/\partial x^2$, $v\,\partial v/\partial y$, $R^{-1}(\partial^2 v/\partial y^2 + \partial^2 v/\partial x^2)$, neglected in (2.6*a–c*) and in §5, may be added to the right-hand sides $\mathscr{L}_n$, $\mathscr{M}_n$. This is done in a passive fashion, in the belief that these extra contributions are not usually part of the dominant physics of the nonlinear unsteady-flow solutions at the Reynolds numbers of real interest. Once again of course the firmest checks available to test this belief are the resulting numerical closeness between the interactive and the full solutions and the extra work required to upgrade the calculations from interactive to full status. The implied additions to $\mathrm{i}\alpha^{-1}\mathscr{L}_n$ are

$$\frac{-\mathrm{i}(n\alpha)^2}{\alpha R} u_n \quad (n \geqslant 0), \tag{6.1a}$$

while $-\alpha^{-2}\mathscr{M}_n$ is supplemented by

$$\frac{\mathrm{i}(n\alpha)}{R\alpha^2}\left[\frac{\partial u_n}{\partial y}-(n\alpha)^2\psi_n\right]-\sum_{m=1}^{n} m(n-m)\,\psi_m\,u_{n-m}$$
$$+\sum_{m=n+1}^{\infty} m(m-n)\,\psi_m\,\hat{u}_{m-n}+\sum_{m=1}^{\infty} m(m+n)\,\hat{\psi}_m\,u_{m+n} \quad (6.1b)$$

for $n \geqslant 1$.

In the test or full calculations, then, the contributions (6.1a, b) were added to (5.3a, c) respectively at each iteration per time level. Otherwise, the discretization and procedures described previously were maintained throughout. The outcome is summarized in figures 3–5. Clearly, raising the computations to full Navier–Stokes status by means of the extra contributions (6.1a, b) produces some quantitative alteration in the results at the values of the Reynolds number studied, but this alteration appears predominantly as a small shift in the temporal period and in the decay or growth rates. This is exactly as the earlier linearized comparisons would suggest, from an inspection of figure 1. Relatively little real change in the amplitude response or in the qualitative properties of the nonlinear unsteady flow is involved otherwise, particularly for the smaller initial amplitudes. A further test on the calculations was also performed here. The component solutions obtained were used to construct the individual terms, u, $\partial u/\partial x$, etc., appearing in the Navier–Stokes equations at particular x-, y-, t-values, and so a measure of how well those equations were satisfied could be derived by substitution. We found that the error relative to $\partial p/\partial x$ decreased from 2% with $N = 5$ components to less than 1% with $N = 7$. Moreover, with these full calculations as compared with the interactive ones there was no significant increase in the number of iterations required for convergence per timestep or in the overall computer time required. This tends to favour the view that the extended interactive boundary-layer approach does indeed provide a quite close approximation to the full solution, numerically as well as physically. Another point of interest here is that from the calculations done so far there seems some evidence of nonlinear effects leading to subcritical instability. Although for $R = 1000$ the initial disturbance amplitudes $A = 1, 5$ (corresponding to 4%, 20% approximate maximum velocity disturbances of the Poiseuille flow) both lead to decay of the nonlinear disturbance A as time t increases, the corresponding decay is much lessened for $R = 3000$, and indeed almost changes to a growth for $A = 5$ then. Slight growth seems evident at $R = 6000$. We note also the slight shift in the temporal period of the response due to nonlinear effects, while for the smaller initial disturbances the temporal period of the unsteady flow solution soon approaches that predicted by linear normal-mode theory.

7. Further comments

The measure of agreement found in §§4, 6 and figures 1–5 between the full (Orr–Sommerfeld or nonlinear Navier–Stokes) results and the alternative (extended interacting boundary-layer) approach, at the Reynolds numbers of most physical interest, tends to add considerably to the value of understanding asymptotic stability properties, we believe. The asymptotic theory points to the dominant physical features of the moderate-to-high Reynolds-number regime, and hence to the dominant terms and balances in the unsteady Navier–Stokes equations. The interactive approach then concentrates on those terms and balances, to construct a numerical

method which, if need be, can be restored readily (§6) to 'full' Navier–Stokes status afterwards, in a perhaps rather novel way, for a reasonably streamlined flow, at least. This seems a fairly powerful application of asymptotic understanding and is, for linear and nonlinear stability, perhaps the most useful to date in real terms for both channel flow and boundary layers.

It would therefore be interesting physically and theoretically to continue the nonlinear unsteady computations, studying other ranges of Reynolds number, wavenumber and amplitude and attempting possible improvements with regard to grid stretching and the introduction of Fourier series, for example, given that the calculations to date appear to have favoured the interactive view taken. The general interactive approach, we should emphasize again, is 'sensible' rather than 'rational' at finite Reynolds numbers (boundary layers for instance do not exist at such Reynolds numbers anyway, strictly speaking), it is open to various interpretations as we have noted before, and it is really concerned more with the application than the theory itself. The present interactive version nevertheless encompasses most of the known features of linear and weakly or fully nonlinear stability theory, and that is to its credit. The occurrence of shorter Rayleigh waves and/or strongly nonlinear critical layers for instance (Bodonyi, Smith & Gajjar 1983) is within the scope. Further, the implied nonlinear aspects of boundary-layer stability have not been investigated yet, nor have the many other possible versions of the unsteady interactive boundary-layer or parabolized Navier–Stokes approach, and these merit further study.

It would be interesting in addition to apply the interactive ideas to other nonlinear unsteady flows of real concern. These include non-parallel flows, such as the motion past a finite flat plate (D. W. Moore 1983, private communication), three-dimensional stability, stratified fluids, and rotating fluids.

Thanks are due to the S.E.R.C., for financial support for D.P. and J.W.E., and for computer support on the Cray at Daresbury.

REFERENCES

Bodonyi, R. J. & Smith, F. T. 1981 *Proc. R. Soc. Lond.* A **375**, 65.

Bodonyi, R. J., Smith, F. T. & Gajjar, J. 1983 *IMA J. Appl. Maths* **30**, 1.

Davis, R. T. & Rubin, S. G. 1980 *Comp. Fluids* **8**, 101.

Davis, R. T. & Werle, M. J. 1982 In *Proc. Conf. Numer. Phys. Aspects of Aerodyn. Flows, California State University, Long Beach, 1981* (ed. T. Cebeci). Springer.

Dennis, S. C. R. & Hudson, J. D. 1978 In *Proc. 1st Intl Conf. on Numer. Meth. in Laminar and Turbulent Flow, University College, Swansea.* Pentech.

Drazin, P. G. & Reid, W. H. 1981 *Hydrodynamic Stability.* Cambridge University Press.

Fornberg, B. 1980 *J. Fluid Mech.* **98**, 819.

Hall, P. & Smith, F. T. 1982 *Stud. Appl. Maths* **66**, 241.

Lin, C. C. 1955 *Theory of Hydrodynamic Stability.* Cambridge University Press.

Messiter, A. F. 1979 In *Proc. 8th US Natl Appl. Maths Congr., Los Angeles.*

Patera, A. T. & Orszag, S. A. 1981 *J. Fluid Mech.* **112**, 467 (see also *Phys. Rev. Lett.* **45** (1980), 989 and *Proc. 7th Intl Conf. Numer. Meth. Fluid Dyn., Paper* 141, *June 1980, Stanford*).

Reid, W. H. 1965 In *Basic Developments in Fluid Dynamics* (ed. M. Holt), vol. 1, p. 249. Academic.

Rubin, S. G. 1982 *Lect. Notes for Series on Computational Fluid Dyn., von Kármán Inst. for Fluid Dyn., Brussels, March/April 1982.*

Schlichting, H. 1933 *Nachr. Ges. Wiss. Gött., Math.-Phys. Kl.* **181**, 208.

Smith, F. T. 1979*a* *Proc. R. Soc. Lond.* A **366**, 91 (and A **368**, 573).

SMITH, F. T. 1979*b* *Mathematika* **26**, 211.

SMITH, F. T. 1981 *J. Fluid Mech.* **113**, 407.

SMITH, F. T. 1982 *IMA J. Appl. Maths* **28**, 207.

SMITH, F. T. & BODONYI, R. J. 1982 *J. Fluid Mech.* **118**, 165.

SMITH, F. T. & GAJJAR, J. 1984 *J. Fluid Mech.* **144**, 191.

STEWARTSON, K. 1981 *SIAM Rev.* **23**, 308.

STEWARTSON, K. & STUART, J. T. 1971 *J. Fluid Mech.* **48**, 529.

STUART, J. T. 1960 *J. Fluid Mech.* **9**, 352.

STUART, J. T. 1971 *Ann. Rev. Fluid Mech.* **3**, 347.

TOLLMIEN, W. 1929 *Nachr. Ges. Wiss. Gött., Math.-Phys. Kl.* **22**, 44 (transl. *NACA Tech. Memo.* 609).

WATSON, J. 1960 *J. Fluid Mech.* **9**, 371.